Experimental investigation of computer-synthesized holograms for generation of ring dark solitary waves and optical vortex solitons

D. Neshev, A. Dreischuh, V. Kamenov, I. Stefanov, S. Dinev, W. Fließer*, L. Windholz*

Sofia University, Department of Quantum Electronics
5, J. Bourchier Blvd., BG-1164 Sofia, Bulgaria

*Technische Universität Graz, Institut für Experimentalphysik
Petersgasse 16, A-8010 Graz, Austria

ABSTRACT

We present experimental results on the evolution of ring dark solitary waves and optical vortices generated by computer-synthesized holograms. The detailed comparative numerical simulations show, that this approach ensures reproduction of the correct intensity and phase portrait of the dark waves at the entrance of the nonlinear medium. The transverse dynamics at both even and odd initial conditions is studied and compared with the theory and simulations.

Keywords: optical vortex soliton, ring dark solitary wave, computer-generated hologram

1. INTRODUCTION

The Ring Dark Solitary Waves (RDSW) in bulk nonlinear media are first introduced and described in the works of Kivshar and Yang [1,2]. In each diametrical slice of the background beam the dark formation appears in the form of two intensity-dips of hyperbolic-tangent profiles spaced at twice the dark ring radius. The phase portrait of the RDSW demonstrates pairs of abrupt π-phase shifts localized at the intensity-minima across the ring. Similar to the one-dimensional and quasi-2D experiments described in [3,4], in the first experimental generation of RDSWs [5] at a pure amplitude modulation at the entrance of the nonlinear medium, pairs of diametrical phase-shifts (less than π) within the dark ring are recorded [6]. In view of the principle possibility multiple signal beams to be guided parallely by RDSWs [7], the improvement of their contrast and the reduction of their transverse velocity is desirable.

The Optical Vortex Solitons (OVSs) could be characterized as localized intensity dips nested in a bright background beam, for which the two-dimensional diffraction is exactly compensated for by the self-phase modulation along the nonlinear medium of a negative nonlinearity. For a first time OVSs are generated by employing the modulational instability of one-dimensional dark formations [8]. Characteristic for these formations are their spiral phase portraits with abrupt π-phase jumps in each radial cross-section. OVSs from controllable initial conditions are generated first by means of Computer-Generated Holograms (CGH) [9].

2. DESIGN OF THE HOLOGRAMS

The desired CGH of an odd dark wave of a circular symmetry should result from an interference between a reference plane wave $I_R(x,y)$ incident at the certain angle θ with respect to an object wave $I_D(x,y) \propto |E_D(r,\varphi)|^2$. In the object wave the dark ring of radius R_0 and width r_0

$$E_D(r,\varphi) = B(r)\tanh\left[(r-R_0)/r_0\right]\exp\{i\phi\} \tag{1a}$$

should be imposed on a background beam B(r). In the above notations φ is the azimuthal coordinate ($\varphi \in [0,2\pi]$), $r=(x^2+y^2)^{1/2}$, and

$$\Phi(r) = \begin{cases} -\pi/2 & for \quad r \le R_0 \\ +\pi/2 & for \quad r > R_0 \end{cases} \tag{1b}$$

represents the diametrical phase jump across the ring dark formation. It is known that only the π-phase jump at the entrance of the Nonlinear Medium (NLM) is able to form a fundamental 1D dark soliton stripe (grid) [4]. This result encouraged us to synthesize CGHs by pure phase modulation of the object wave.

The interference pattern obtained by using the well known relation

$$I(x,y) = I_R(x,y) + I_D(x,y) + 2\sqrt{I_R(x,y)I_D(x,y)}\cos(\frac{2\pi}{\lambda}x\cos\theta + \Phi) \tag{2}$$

is shown in Fig.1. The real CGHs, however, were produced photolitographically at a grating period of 20 μm on 15x15 mm^2 optical glass substrates.

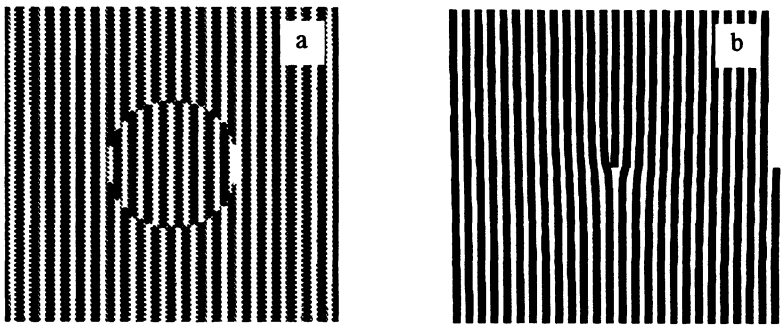

Fig. 1. Computer-generated holograms of a ring dark wave a) and optical vortex b) obtained at a pure π-phase modulation in the object beam.

Following the classification of the CGHs [10], the discussed ones are of binary transmittance. At equal widths of the transmissive and reflective stripes (Fig.1) it is shown analytically [13], that the even diffraction orders (except this with m=0) should disappear. In our case the diffraction efficiency at the first orders was estimated to be 8.5%, close to the 10% limit predicted [10].The diffraction efficiency in the even orders was negligible (Fig. 2a). Figs.2b,c demonstrate two ring dark formations of different radii reconstructed from CGHs (in the $\pm$1-st diffraction orders) and the zero order transmitted beam. Since the interference structure was quantized in two discrete levels, an irreducible quantization noise was added to the reconstructed wavefronts. According to [10], however, the mean square error was down to $\pi/24$.

3. PHASE MEASUREMENTS OF THE 2D RING DARK FORMATIONS REPRODUCED FROM THE CGHs.

In the first step of the CGH reconstruction-analysis we measured the transverse phase-shift of the ring dark formation generated. Interference was obtained in a Mach-Zehnder interferometer (Fig. 3) formed by a beam-splitter BS1, the mirrors M2 and M4 and the beam-splitter cubes C1 and C2. For a purpose of a controllable optical path-length variation, a Michelson interferometer (BS2, M3, M4) was built-in in its reference arm. The path-length was changed by the piezoceramic-transducer mounted mirror M4 and sensed by the variations in the interference pattern in the Michelson interferometer via the photodetector D. The telescope T1 was used to adjust the spatial frequency of the interference pattern at the detector plane, whereas the telescope T3 matched the reference and object beam cross-section. Two filter sets F1 and F2 were used to avoid CCD-camera saturation at a direct CCD-array illumination and to control the interference pattern contrast. This arrangement has made possible to record sets of three interference pictures at known phase shifts (0, $2\pi/3$, $4\pi/3$) per exposure and, thereafter, to reconstruct the 2D phase portrait of the dark formation by the three-frame technique [11,6].

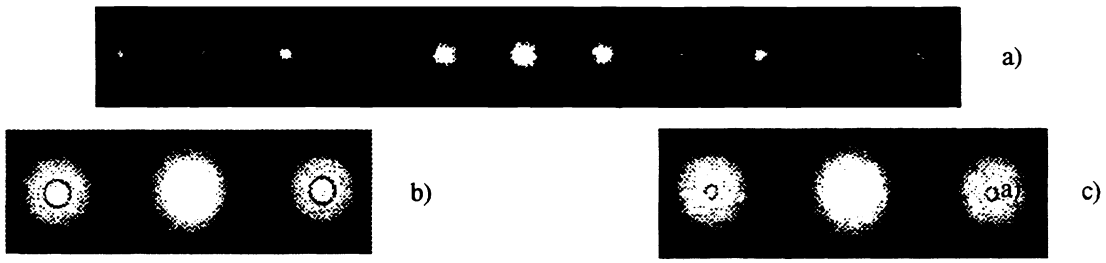

Fig. 2. Overview CCD camera images of some of the diffraction orders (a) and zero and $\pm$1-st diffraction orders of two ring dark formations (b,c) of different radii reconstructed from different CGHs.

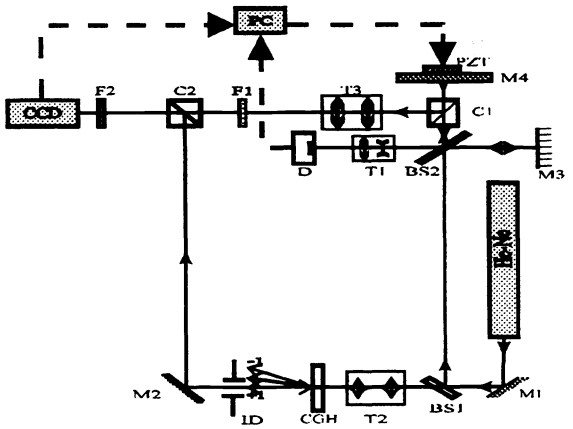

Fig. 3. Experimental setup used in the phase measurements (M1, M2, M3-mirrors; M4 and PZT-piezoceramic mounted mirror; BS1, BS2 - beam-splitters; T1, T2, T3-telescopes; C1, C2 - beam-splitter cubes; D-detector; F1, F2-filter sets; CGH-computer generated hologram; ID-iris diaphragm; PC- personal computer; CCD- camera)

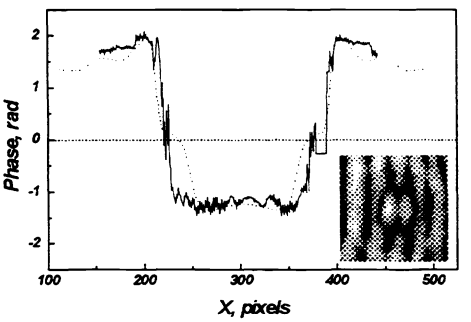

Fig. 4. Diametrical phase distribution of a ring dark formation reconstructed from CGH (solid line). Dotted line - numerical result obtained at $z=45\,L_{Diff}$ and $R_0/r_0 = 14$. Insert - grayscale image of one of the interference patterns used in the tree-frame method for phase distribution retrieval.

In Fig.4 we present the experimental phase distribution across a dark ring of 2 mm diameter reconstructed form the CGH located 175 cm away from the CCD camera. The grayscale image inserted shows the system of interference lines used in this measurement. The phase-distribution presented is evaluated along the interference lines. Pairs of opposite phase shifts of nearly π are clearly seen. One can see weak distortions in the abrupt phase changes at the phase-level denoted as zero and at the bottom of the phase step. We attributed these deviations to a diffraction of the dark ring.

The linear 2D evolution (diffraction) of optical beams along their propagation path could be described in a natural way by solving the (2+1)-dimensional nonlinear Schrödinger equation (NLSE) [1,2]

$$i\frac{\partial E_D}{\partial z} + \beta\left(\frac{\partial^2}{\partial x^2} + \frac{\partial^2}{\partial y^2}\right)E_D + kn_2\left|E_D\right|^2 E_D = 0 \qquad (3)$$

at $n_n = 0$.

In Eq.3 the term comprising $\beta = (2k)^{-1}$ accounts for the beam diffraction and $n_2\left|E_D\right|^2$ is the medium refractive-index correction due to the presence of the intense beam inside the NLM (if present). In the linear reconstruction analyses (at n_2=0) Eq.3 was solved numerically over 1024 x 1024 grid points. Closest agreement between the experimental (Fig.4a-solid line) and numerical results (dotted line) was found at $z=45\,L_{Diff}$ for R_0/r_0=14, where L_{Diff} is the Rayleigh diffraction length. The results indicates that the phase-variations at the half-high of the jump and at the phase-minimum results from the unavoidable diffraction. This was confirmed by placing the CGH 60 cm in front of the CCD camera. At this location the agreement between the experimental and numerical data was gradually better.

We investigated the intensity distribution of the generated dark formation and good agreement with the theory was obtained.

Two particular conclusions could be drawn from the CGH reconstruction and from the simulations:

i) At suitable distances the binary transmittance holograms generated at a pure phase modulation reproduce the π-phase jump encoded;

ii) The intensity modulation of the dark ring is adequately described by hyperbolic-tangent profile.

4. TRANSVERSE DYNAMICS OF RDSWs

The experimental arrangement for measuring the evolution of RDSWs radius R_0 and width r_0 along the nonlinear propagation path is shown on Fig.5. The 514.5 nm line of a multiline Ar ion laser of a power of 300 mW was used to reconstruct the CGH and the diameter of the first diffraction order beam at the entrance of the NLM of length 5cm was

reduced to 200μm by a telescope. A pair of two identical prisms, one of them immersed in the nonlinear liquid (hydrocarbon oil 'Nujol'-Merck, dyed with $SPC_{16}6(NO_2)$ to a molar concentration of $1.1.10^{-3}$Mol) provides the possibility to couple the background beam and the RDSWs out of the cuvette at variable length of the nonlinear propagation path. Under this conditions the maximum nonlinear propagation length inside the cuvette was limited to 3.2 cm and the maximum nonlinear refractive-index change was $\left|\Delta n_{\max}^{NL}\right| = 4.10^{-4}$. The eventual saturation of the CCD camera located at 21 cm after the exit of the NLM was prevented by suitable filter-sets F (Fig.5).

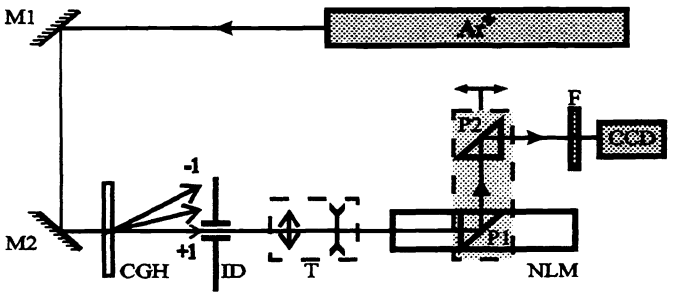

Fig. 5. Experimental setup used for measuring the RDSW dynamics (Ar^+-argon ion laser; M1, M2-mirrors; CGH-computer generated hologram; ID-iris diaphragm; T-inverted telescope; NLM-nonlinear medium; P1, P2- 90°-prisms on a translation stage; F-filter set; CCD-camera)

All further numerical simulations in this work are based on solving the NLSE (Eq.3) by the split-step Fourier method over 1024x1024 grid points under self-defocusing conditions ($n_2<0$). The initially 'black' RDSW at the entrance of the NLM was modelled according to Eqs.1a-b. In the nonlinear medium the longitudinal coordinate z was naturally to be expressed in units of nonlinear lengths $L_{NL} = (k|n_2|A_0^2)^{-1}$, where A_0 is the amplitude of the background beam B(r).

As a second step we analysed both numerically and experimentally the dynamics of RDSWs of equal widths r_0 and different radii R_0, generated with odd initial conditions. Fig.6 presents numerical results intended to clarify as far the analytical results on the RDSW radius R_0 vs. z obtained in [1] match the solution of the NLSE. The adiabatic approximation used in [1] is found to influence gradually the small rings only, whereas at $R_0>6r_0$ the numerical results (dashed curves) are practically identical to the analytical ones (solid curves).

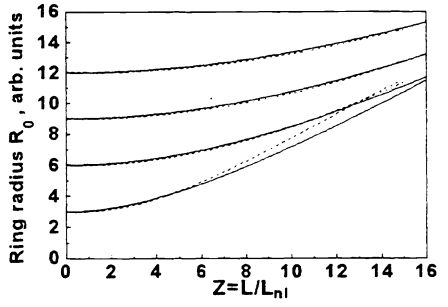

Fig. 6. RDSW radius R_0 vs. normalised nonlinear propagation distance z at different values of $R_0/r_0 = 14$ (solid curves-analytical results following [1], dashed-numerical solutions of the NLSE)

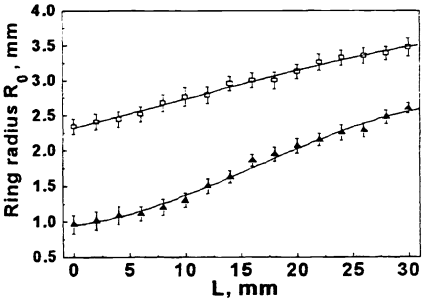

Fig. 7. RDSW radius R_0 measured at the CCD-camera plane vs. nonlinear propagation path-length L at $R_0(z=0) = 12.5\mu m$ (lower curve) and $R_0(z=0) = 85\mu m$ (upper curve) at the entrance of nonlinear medium. The bars indicate the measured values of the ring width r_0.

The experimental results on the evolution of RDSWs obtained with CGHs (Fig.7) confirm, that the initially larger R_0 is, the weaker expressed the dynamics of the dark formation along the NLM is. The bars in Fig.7 present the measured ring-widths r_0 along the propagation path. The decrease of the width r_0 in the RDSW with the smaller radius and the weak change of the curvature of the dependence are results of both the higher transverse velocity of this formation inside the NLM, and the diffraction from the side-lying exit of the cuvette to the CCD camera.

5. PHASE MEASUREMENTS OF OPTICAL VORTICES REPRODUCED FROM THE CGHs.

As a second step of our measurements we investigate the phase distribution of a single optical vortex reconstructed from the CGH shown in Fig.1b. When the telescope T3 (Fig.3) was detuned the reference beam of a spherical wavefront yields at the output plane spiral phase-pattern (Fig.8a). By adjusting the telescope T3 the interference stripes are parallel. One can see the well known splitting of the interference stripe in the centre (Fig.8b). From this pattern we extracted the phase distribution of the reconstructed optical vortex. It is presented at Fig.9a. Despite of the relatively strong optical good agreement with the calculated phase distribution (Fig.9b) could be observed.

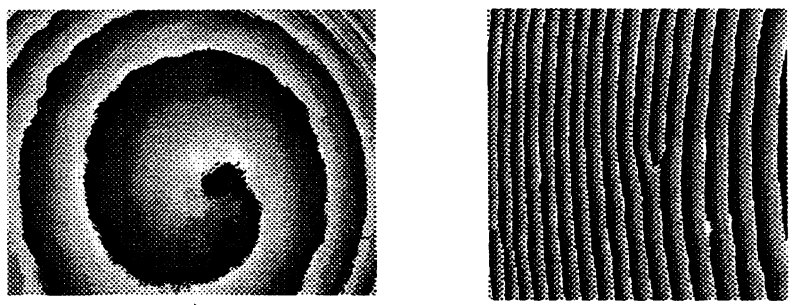

Fig. 8. Experimental obtained phase distribution of the interference pattern of a single vortex, recorded with a spherical (a) and plane wavefront (b).

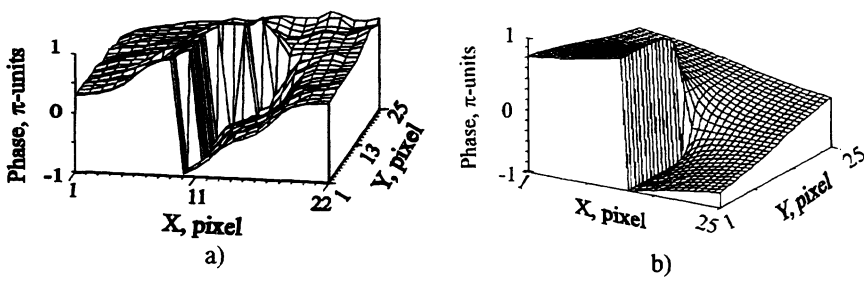

Fig. 9. Phase distribution of single vortex ((a) - experimental result; (b) - theory).

We have investigated the phase distribution of the close placed vortices with equal or opposite topological charges. In this case we again obtained good agreement with measured phase distribution and calculated one.

6. MULTIPLICATION OF CGHs

For generation of more complicated intensity and phase profiles on common background beams we investigate the case when two CGHs are put together and the second one is rotated at 90° with respect to the first one.

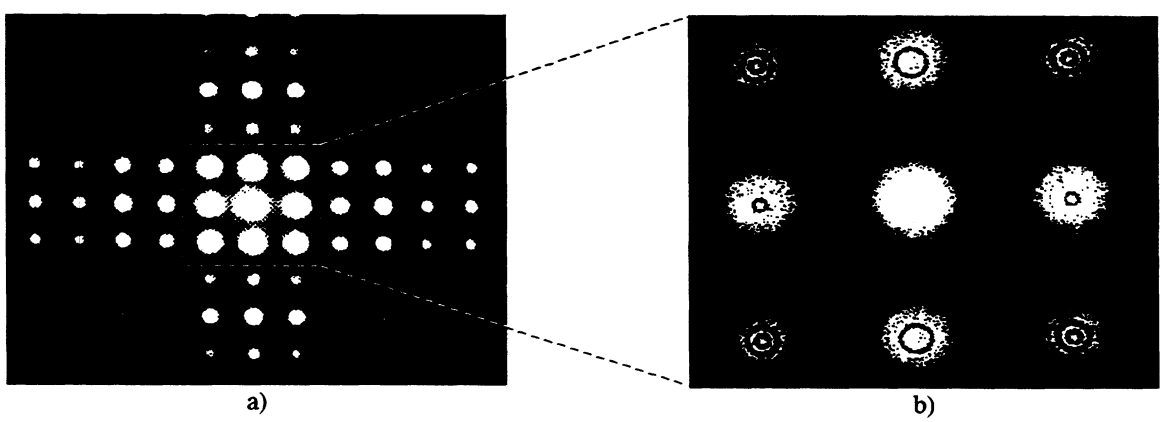

Fig. 8. Overview CCD camera images of some of the diffraction orders when two CGHs are placed together and the second one is rotated at 90° relatively to the first (a) and zero and ± 1-st diffraction orders of two ring dark formations (b) reconstructed from such multiplication of the two CGHs.

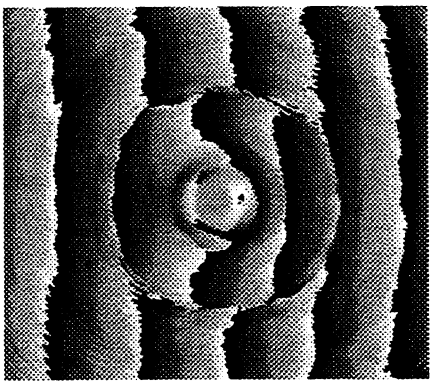

On this way one can obtain much more complicated diffraction picture. When two CGHs for reconstruction of ring dark formations are used the diffraction orders are shown at Fig.8. In the vertical and horizontal direction we still have simple diffraction orders, but in the diametrical direction we have multiplication of the two dark formation. The measured phase interference pattern is shown at Fig.9. Similar situation was observed when two CGHs, one of a ring dark formation, the second - of an optical vortex reconstruction, are used.

Fig.9. Phase distribution of the interference pattern of a configuration of two coaxial rings

7. CONCLUSION

In view of the above analyses we are convinced to state, that the reproduction of computer generated holograms of binary transmittance generated at a pure phase modulation of the object wave are able to ensure adequate intensity and phase-distributions for the generation of initially black dark solitary waves. The ring dark formation generated on this way demonstrate reduced dynamics as compared to the RDSWs generated by an amplitude modulation of the background beam. Such CGH can be used for generation of optical vortex solitons which posses good guiding properties and are stable with respect to laser power fluctuations and perturbations.

8. ACKNOWLEDGEMENTS

The Bulgarian co-authors would like to thank the Technical University Graz, Institute of Experimental Physics, for the warm hospitality during their research stays. D.N. and V.K. were BMWFK-fellows. A.D. was a fellow of the Österreichischer Akademischer Austauschdienst. This work was supported partially by the CEEPUS-project (Network A-21) and by the National Science Foundation, Bulgaria.

9. REFERENCES

1. Yu. Kivshar, X. Yang, "Ring dark solitons," *Phys. Rev.* **E50**, R40-R43 (1994); ibid., "Dynamics of dark solitons," *Chaos, Solitons & Fractals* **4** 1745-1758 (1994).

3. D. Andersen, D. Hooton, G. Swartzlander, Jr., A. Kaplan, "Direct measurements of the transverse velocity of dark spatial solitons," *Opt. Lett.* **15**, 783-785 (1990).

4. G. Swartzlander, Jr., D. Andersen, J. Regan, H. Yin, A. Kaplan, "Spatial dark soliton stripes and grids in self-defocusing materials," *Phys. Rev. Lett.* **66**,1583-1586 (1991).

5. S. Baluschev, A. Dreischuh, I. Velchev, S. Dinev, O. Marazov, "Odd and even two dimensional dark spatial solitons," *Appl. Phys.*, **B61**, 121-124 (1995); ibid., "Generation and evolution of two dimensional dark spatial solitons," *Phys. Rev.* **E52**, 5517-5523 (1995).

6. A. Dreischuh, I. Velchev, W. Fließer, "Phase measurements of ring dark solitons," S. Dinev, L. Windholz: *Appl. Phys.*, **B62**, 139-142 (1996).

7. A. Dreischuh, V. Kamenov, S. Dinev, "Parallel guiding of signal beams by a ring dark soliton," *Appl. Phys.* **B63**, 145-150 (1996).

8. G. Swartzlander, Jr., C. Law, "Optical vortex solitons observed in Kerr nonlinear media," *Phys. Rev. Lett.* **69**, 2503-2506 (1992).

9. B. Luther-Davies, "Nonlinear rotation of 3D dark spatial solitons in a Gaussian laser beam," *Opt. Lett.* **19**, 1816-1818 (1994).

10. W.-H. Lee, "Computer-generated holograms: Techniques and applications," *Progress in Optics* **XVI**, 119-232 (1978).

11. C. Creath, "Temporal Phase Measurement Methods" in *Interferogram Analysis*, ed. by D. Robinson, G. Reid (Inst. of Physics, Bristol 1993), pp. 94-140.